International Journal on Interactive Design and Manufacturing (IJIDeM)
https://doi.org/10.1007/s12008-023-01729-3

ORIGINAL ARTICLE

Microstructural evolution and the effect of electron beam melting on the fatigue characteristics of 7075 Al alloy deposited by MIG arc additively manufacturing

Irina Panchenko[1] · Suresh Gudala[1] · Dmitrii Labunskii[1] · Sergey Konovalov[1]

Received: 1 August 2023 / Accepted: 15 December 2023

Abstract
The current investigation was carried out to study the microstructural and mechanical characteristics of the AA7075 fabricated part by MIG arc additive manufacturing. It was observed that primary columnar grains and fine secondary phases form along the grain boundaries to generate the solidification structures. Grain refining and particle uniform distribution were discovered to be responsible for the increased mechanical characteristics. The porosity of the samples was found to be less than 2%. The microhardness of the samples was found to increase with layer depth in the fabricated part. Comparatively, the average fatigue strength of the bottom region samples increases by 16% compared with the other samples. The marginal increase in fatigue strength is mainly caused by the formation of strengthening mechanisms due to the lower temperature gradient. The fatigue fracture propagation behavior of fabricated parts was primarily influenced by dented plastic zones and stress concentrations produced by impact-induced geometric changes. The reduced life of the fabricated part close to the middle region was primarily due to tensile residual stress, leading to early fatigue crack initiation. The fatigue performance of the fabricated part near the bottom region is attributed to the increase in surface hardness and beneficial compressive residual stresses. Electron beam melted fatigue tested samples sustained a greater number of cycles due to the refinement of fine to coarse precipitates, with crack initiation from the surface and crack propagation occurring with fatigue striations.

Keywords AA7075 alloy · MIG arc additive manufacturing · Microstructure · Phase analysis · Microhardness · Fatigue analysis

1 Introduction

Aluminum and its alloys are widely used in marine industries, aircraft manufacturing, shipbuilding, automobile body components, and other structural applications. They have excellent strength-to-weight ratio, ductility, and corrosion resistance [1, 2]. Comparatively, aluminum has a relatively lower strength than many steels, which limits its applications in many industries. However, adding the alloying elements, heat treatments, and nanofillers to the components strengthen the components, thereby improving their overall performance and life. In recent years, aluminum alloys have drawn much attention from researchers due to their improved mechanical properties like specific strength, density, wear, fatigue resistance, and thermal expansion. Among all aluminum alloys, the 7000 series constitutes the preferred group of materials in the aviation, space, and military industries owing to their higher strength. The preferred group of industrial alloys of the 7000 series mainly contain zinc, magnesium, and copper, with minor quantities of manganese, chromium, and zirconium to control grain growth during recrystallization. In the aerospace and automotive sectors, the Al 7000 series was mainly used due to their better strength and machinability characteristics, possibly due to zinc as the primary alloying element. In commercial 7075 Al alloys, fatigue cracks nucleate at the surface where intermetallic particles or inclusions occur [3]. In many cases, silicon impurities influence the reduction of fracture toughness and fatigue strength. Improvements in mechanical performance at higher loads are required in cyclic load-bearing components of many engineering applications. Earlier, a few studies focused on the structure and properties of aluminum alloy

✉ Sergey Konovalov
konovalov@sibsiu.ru

[1] Siberian State Industrial University, 42, Kirova Street, Novokuznetsk, Russia654007

Published online: 30 January 2024

by ion implantation [4], shot peening [5], electron beam processing [6, 7], vibratory stress relief [8], and by depositing various coatings [9–14].

Additive manufacturing (AM) is revolutionizing the industry due to its higher efficiency and flexibility for mass production. In recent years, AM technologies have gained much attention due to their multiple features, like their high degree of freedom, net formation, and high degree of research and development. As repeated thermal cycling during the fabrication of layers occurs in the deposition process, a complex heat effect can be experienced at the local microstructure. The development of multiscale microstructures is common. Compared with conventional subtractive methods, additive manufacturing offers attractive benefits like complex shape production, lower cost, rapid processing time, etc. Mainly, three AM methods are widely used for metallic materials: arc welding, laser, and electron beam. The laser-based process has high precision but very pool energy efficiency. Electron beam-based processes have higher energy efficiency, but the requirement of a high vacuum environment limits their applications. Later, arc welding was studied for AM of components due to its low processing cost and time. The common AM methods based on arc welding are divided into the following groups: tungsten arc welding (TAW), plasma-transferred arc welding (PTA), and metal arc welding (MAW). In the MIG process, the produced arc was struck between the wire, the substrate material, and the following layers. Due to the electric arc, wires will be melted and formed as layers at a higher deposition rate, which is beneficial for building large three-dimensional metal parts. Earlier, research studies based on automated MAW were developed for fabricating three-dimensional structures [15, 16]. Then increase the frequency of the droplet in order to improve the forming quality [17]. In order to improve the quality, Kim et al. [18] focused on optimizing welding parameters using regression analysis and neural networks in the joining applications. Also, a few studies focused on combining MIG and metal active gas (MAG) with the integration of CNC (computer numerical control) in order to manufacture metallic dies and molds [19]. The GMAW-based AM process can also be implemented with milling and hybrid milling and welding, subsequently increasing the surface quality. Xiong et al. studied the materials and energy saving while changing the deposition velocity with a passive energy sensor in MAW [20, 21]. Few studies focused on the forming characteristics of double electrode MIG developed thin parts [22]. As the heat input is an important process parameter for deposition efficiency, optimum control of the heat input is necessary. However, the stability of the MIG could be more accurate. The accumulation of heat developed due to the MIG arc will increase with the number of layers in the AM. It may affect the dimensional accuracy and surface quality, limiting the MIG utilization of AM parts. However, control of the process parameters of the MIG process would give better results for AM-developed parts. The literature shows that deposited samples with a fine microstructure have inferior mechanical characteristics compared to heat-treated materials. Few researchers investigated the various post-heat treatment methods for increasing microstructural and mechanical characteristics [23–27]. Among those, electron beam melting has significant advantages due to its capacity to achieve superior grain refinement and homogeneity compared to other approaches [28, 29]. The depth of surface modification increases with an increase in beam energy density. However, few researchers have studied the impact of beam energy density on microstructural and mechanical properties. At lower beam energy density, the surface morphology is relatively uneven and extends into the depth of intergranular cracks [30]. Although the phase composition is not much affected, crystallization and tensile strength are optimized at lower beam energy density (10 J/cm^2). As the beam energy density increases, the depth of surface modification also increases, but the depth of intergranular cracks reaches its maximum value [31, 32]. The additive manufacturing (AM) technologies are still emerging, and we still need to fully understand how the high solidification rates and thermal gradients involved in AM processing affect materials. Additionally, there have been few studies on the effects of post-processing using electron beam melting of AA7075 alloy fabricated using AM, and how it impacts the material's microstructure and mechanical properties still needs to be discovered. The manufacturing industry requires innovative technologies for better design and manufacturing. To address the challenges faced in this industry, effective and scalable solutions are needed for better collaboration and coordination in manufacturing across the product life cycle. The aim of this study was to develop AA 7075 alloy using a MIG arc additive manufacturing method to enhance its microstructural and mechanical properties as compared to traditional techniques. The produced AA 7075 alloy was then subjected to electron beam irradiation, which resulted in improved hardness and fatigue analysis. In addition, MIG arc additive manufacturing was explored for the development of discrete objects. Various software tools were used to analyze the microstructural and mechanical properties of the AA 7075 alloy and to enhance the process outcomes. Additionally, different computing software programs were employed to choose the optimal electron beam irradiation process parameters and evaluate their effects.

Hence, the present study is devoted to studying the microstructure and fatigue analysis of additively manufactured Al7075 parts developed by an optimized MIG process. Further, specific microstructure details of fractured parts in different layers are analyzed and explored. Further, the electron beam melted samples' fatigue life was studied for their potential use in cyclic loading applications.

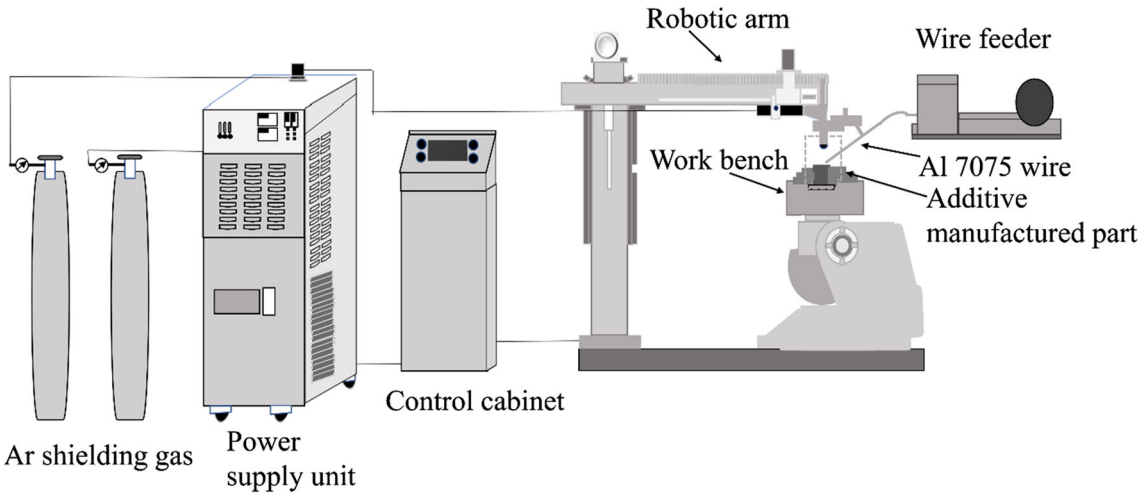

Fig. 1 Schematic representation of part fabrication by MIG arc additive manufacturing

Table 1 Chemical composition of the wire and deposited layer

Type	Weight percentage (wt%)							
	Al	Fe	Mn	Cu	Mg	Cr	Zn	Ti
Wire	88.87	0.1	0.3	1.6	2.51	0.18	6.02	0.02
Layer	86.08	0.27	0.47	2.8	2.15	0.18	8.05	–

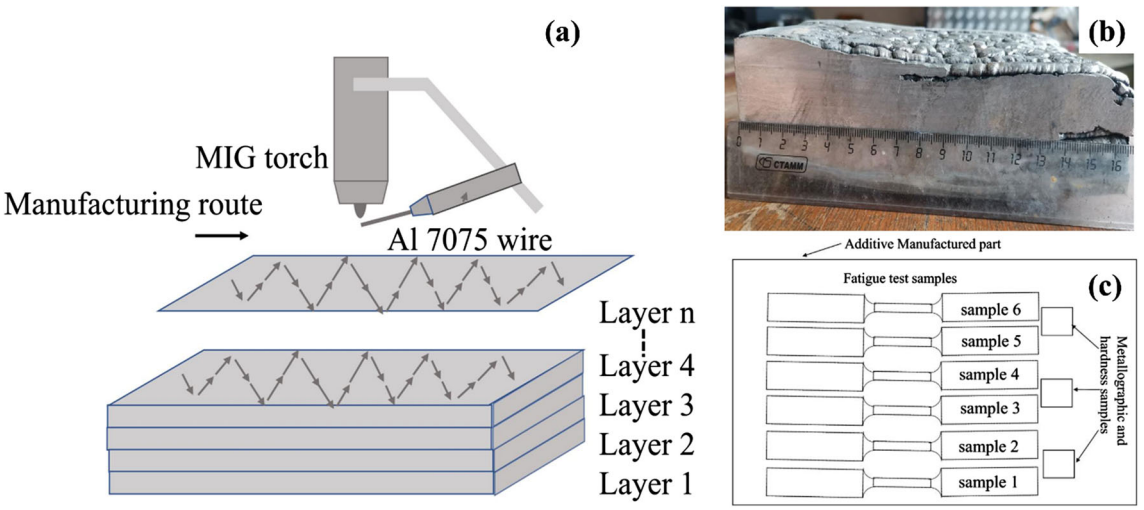

Fig. 2 **a** Schematic illustration of deposition **b** Fabricated sample **c** sampling fashion for fatigue test and metallographic analysis

2 Materials and methodology

Figure 1 shows the schematic representation of the part fabrication by MIG arc additive manufacturing. The MIG/MAG arc welding machine (AMIG500) was utilized to fabricate the part layer by layer. The Al7075 aluminum wire of 1.2 mm diameter was fed to form the layer deposition on the aluminum alloy plates with dimensions of 100 mm × 100 mm × 6 mm. Ar (95%) and CO2 (5%) were applied to the MIG welding torch with a flow rate of 20 L/min. The wire feed rate is 6.1 m/min, 15.6 V voltage, and a current of 130–140 A was maintained throughout the process. The nominal chemical composition of the wire and deposited layer is shown in Table 1. The deposition of layers was carried out slowly on the welding plate with the optimum MIG parameters. The torch angle with the substrate was kept constant during the deposition of all layers. The temperature between the layers was maintained and controlled at 100 °C. The deposited layers were 100 mm in length, and the fabricated

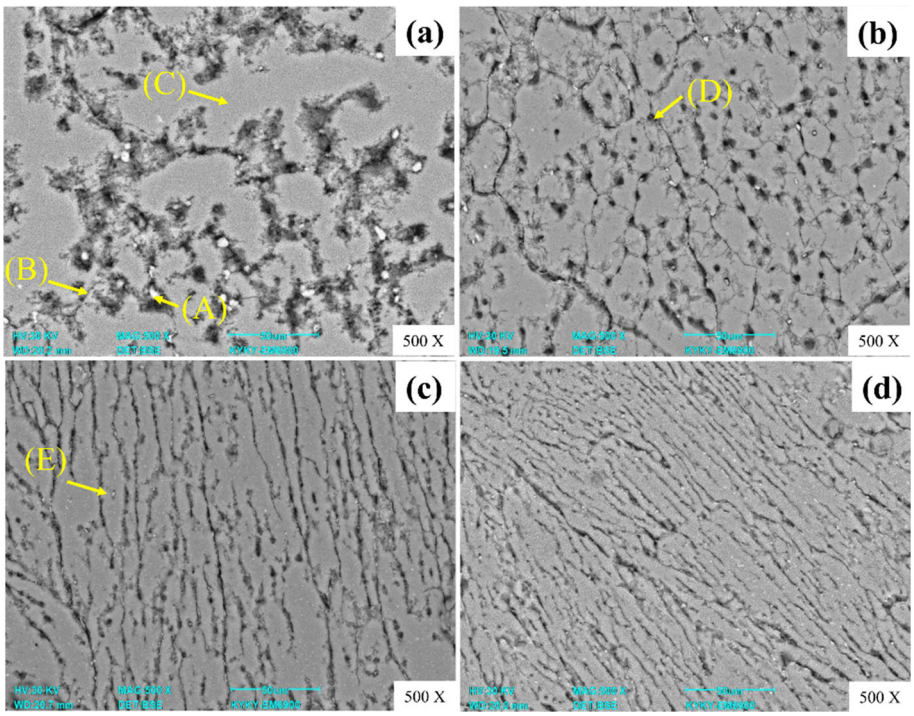

Fig. 3 Microstructure of the part using Al7075 wire **a** top region **b** middle region **c** area above the bottom region **d** bottom region

part was a combination of 15 layers. The schematic representation of deposition was shown in Fig. 2a. The fabricated part with 15 layers of deposition is shown in Fig. 2b. Then the samples were cut into cross-sections using the DK 7732 M11 machine, cleaned with acetone, and etched with reactants: 1.5 mL HF and 3.5 mL distilled water. The sampling fashion for metallographic tests, microhardness and fatigue analysis was represented as a schematic in Fig. 2c. Later, the samples were polished with emery papers of 500, 800, 1000, and 2000 grades. The cross-section of the samples was observed using a scanning electron microscope (KYKY-EM6900). The microhardness of the samples throughout the thickness of the fabricated part was carried out using a Vickers microhardness tester (HVS-1000 A) with a load of 100 gf and a dwell time of 10 s. The XRD analysis was carried out to determine the crystal structure of the deposited layers with a Shimadzu XRD-6000 unit. The fatigue samples were cut vertically to the welding line according to ASTM E8. The fatigue analysis was further studied using an asymmetric cantilever bending setup. Later, few fatigue test samples are remelted using an electron beam melting process (Arcam EBM) at a constant accelerating voltage of 60 kV and the optimum current and voltage.

3 Results and discussions

To understand the microstructure of fabricated part, SEM images of etched samples were taken, and the morphology of the top, middle, and bottom regions are shown in Fig. 1. Fabricated parts are shown to have a dense and uniform structure without visible defects or cracks. The forming dimensional features, including width, height, and deposited dimension, were measured using a vernier caliper. The deposited part's height and width are 165 mm and 8 mm, respectively. No traces of solidification cracks were observed, and the average percentage of porosity was observed to be less than 2%. During the fabrication of the x + 1 layer, the top region of the x layer was remelted, resulting in the formation of the interface layer. As this region has a higher cooling rate due to interlayer cooling, larger and equiaxed structures are formed (Fig. 1a). Above the inter-layer or middle region, a mixing structure of columnar and dendritic equiaxed structures was formed because of the lower thermal gradient (Fig. 1b). Based on the heat accumulation effect, heat dissipation becomes lower with the increase in part height, resulting in a decrease in the thermal gradient. Pure equiaxed grains were formed of 80–200 μm height near the top region of the solidified layer. The columnar grain structure was obtained near the interlayer or bottom region, which is attributed to the lower heat dissipation. During the fabrication of layer by layer, columnar and equiaxed crystals are formed alternatively near the interlayer boundary. The morphology of the grains was good, with a minor percentage of porosity. The grains formed in the deposited layer have well defined grain boundaries indicating the alloy precipitation of secondary phase. This inhomogeneous second phase was formed around the grain boundaries,

Table 2 EDS analysis of different regions in Fig. 3

Region	Composition (wt%)					
	Al	Fe	Mn	Cu	Mg	Zn
A	94.18	–	0.28	0.35	3.19	1.73
B	92.74	0.22	0.47	0.85	3.20	2.09
C	94.12	–	0.38	0.46	3.14	1.71
D	93.52	–	0.18	0.84	2.32	3.00
E	92.71		0.20	1.14	2.25	3.24

which can be dissolved during repeated heating in the fabrication process. A lower percentage of the undissolved second phase was obtained near the top and middle regions than the bottom region, indicating less heat action. The secondary phases are not well dissolved into the metallic matrix. The precipitates formed in the part were smaller than 250 nm. The top region of the sample, Fig. 3a reveals a large amount of secondary phases on the grain boundary. These phases are mainly composed of $MgZn_2$ precipitates. These precipitations are further impeding the movement of grain boundaries. These precipitations are dissolved in the middle and bottom regions due to the lower thermal gradient (Fig. 3b–d). The secondary phase particles were slowly dissolved and mixed well with the Al matrix. To identify the chemical composition of different phases in top, middle and bottom region of the sample, EDS analysis was conducted and the results of the chemical composition at various locations in Fig. 3 was presented in Table 2. In terms of grain size, larger equiaxed grains were produced near the bottom region than the top and middle regions due to the repeated heat action. These microstructural transformations during deposition may have an impact on mechanical properties. The grain morphology changes as the layer thickness changes, and columnar grains predominate. A few equiaxed grains occur along layer boundaries. Although there is no appreciable change in grain size, the microstructure close to the surface still exhibits some degree of equiaxed crystal shape. The arch-shaped surplus weld bead region has high levels in the center and low levels on both sides. Furthermore, the grain size and form are not greatly altered in HAZ, either in the top or bottom regions. There was significantly less heat from subsequent layers near the inter-layer region. A layer-type structure with a thickness of roughly 0.3 mm is already present beneath the top melting pool.

Defects in Al7075 MIG arc deposits can be classified as material-related or process-related. Process-related defects include inhomogeneous microstructure, deformation, and residual stresses, whereas materials-related defects include porosity, oxidation, and solidification cracking. The deposits undergo non-uniform temperature cycles during MIG arc fabrication of the part, resulting in a wide variation of grain morphology, which further affects the mechanical characteristics due to inhomogeneity [33].

The elemental mapping of the bottom region is shown in Fig. 4a. It can be seen that Al, Mg, Zn, Cu, and O are well distributed. The EDS spectra show a minor amount of O, indicating the formation of oxides. The phases in the Al alloy and their second phases are brittle and rigid (Fig. 4b). Due to this, the plasticity of materials rises with a decrease in coarse second-phase particles, which reduces the cracking issue in the fabricated parts [34]. The distribution of elements in the alloy, the thermal gradient, and the type of treatment usually influences the microstructure, corrosion, and tribological properties [35–37]. It has been shown that precipitates are formed due to the Mg and Cu near the grain boundary with the Al grains. The grain size has been shown to vary with the width of the fabricated part. Heat input may influence grain formation and shape. The results showed that the presence of Cu in the 7075 Al alloy would increase the thermal gradient. That results in a decrease in dendrites and columnar grains in equiaxed crystals. The component's fatigue life can be estimated with constant and varied amplitude loading. A few mechanical properties can be improved by strengthening the surface properties of aluminum alloy. The formation of various phases in AMed samples was analyzed using X-ray diffraction (Fig. 5a). It was observed that the main phases were found to be Al and Cu_3Ti_3O.

The microhardness of the fabricated Al7075 part across the width is shown in Fig. 5b. It can be seen that the microhardness of the top layer was found to be 100 HV0.1. With the increase in the layer's width, the microhardness of the part decreased. The microhardness of the middle layer was found to be in the range of 95–88 HV0.1. Due to the higher cooling rates in the bottom region, the average microhardness of the components in the bottom region was greater than that of the top and middle regions. More indentations were performed on the samples along their length and breadth to determine the distribution of hard phases. A contour plot was created by indicating microhardness values at various locations (Fig. 6). The hardness representation was shown in scale (blue to red). It can be seen that more hardness zones are present in the bottom region than in the top and middle regions, indicating the formation of hard phases. The middle region has the lowest hardness among the three regions due to intermediate cooling. The fatigue test samples conducted near the top, bottom, and bottom regions are shown in Fig. 7. Samples 1, 2 were taken from top region, 3 and 4 samples were taken from middle region, and 5 and 6 samples were taken from bottom region. As shown in Fig. 7, the fatigue life of both as-deposited and electron beam melted specimens near the top, bottom, and center regions was analyzed, and the sustainability of each specimen before failure was observed. It was found that the middle region sample only sustained a

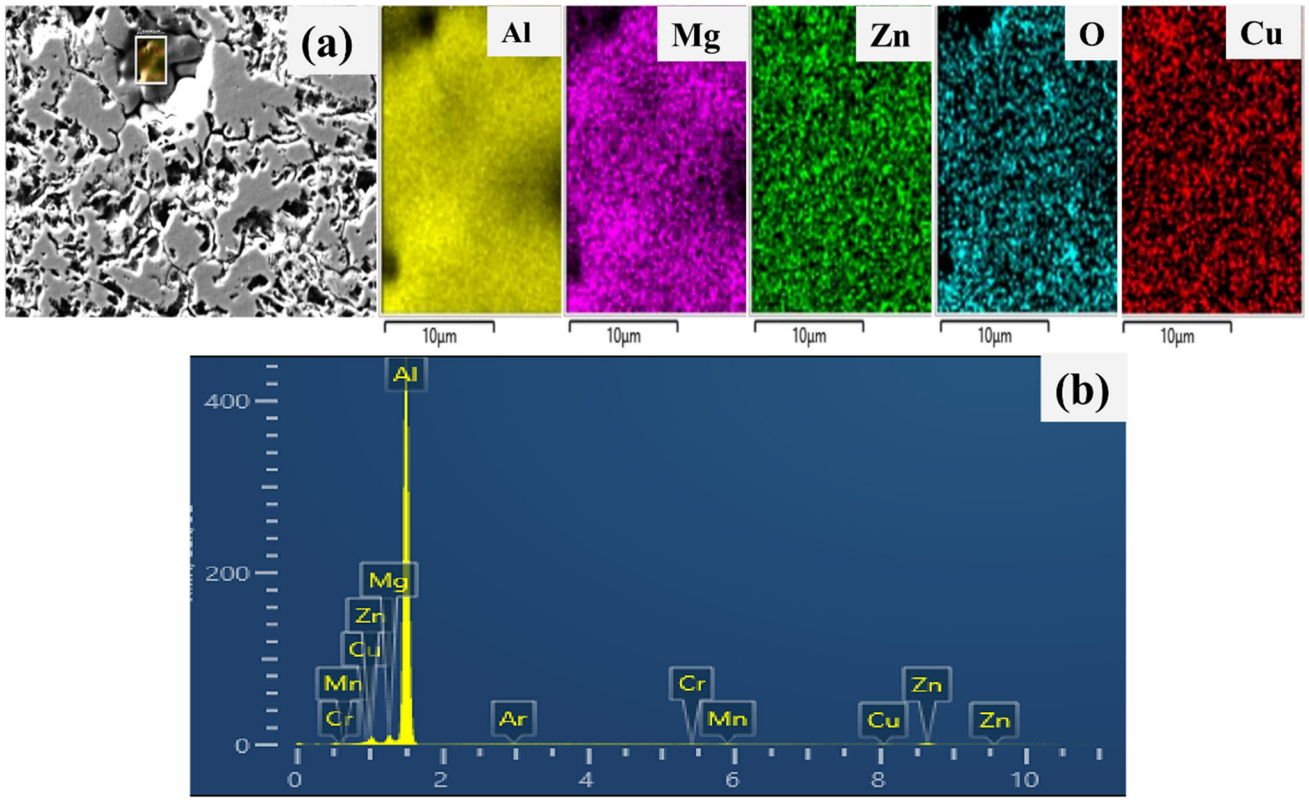

Fig. 4 **a** Elemental mapping of fabricated part near bottom **b** EDS spectra

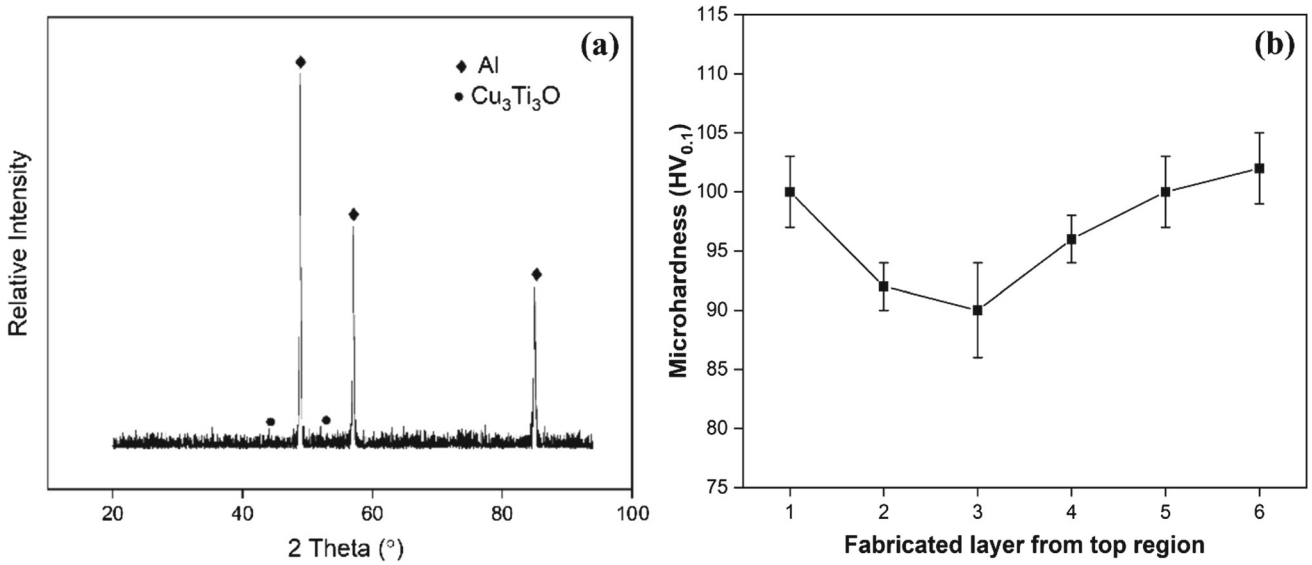

Fig. 5 **a** XRD anslysis of depsited AM part **b** Microhardness of the fabricated part on each layer

limited number of cycles. The sample extracted near the bottom portion appeared to have more cycles than the others. This could be due to grain refinement and a change in heat input. The formation of phases due to secondary inclusions results in the formation of cracks. It can be noted that cracks arise primarily due to the formation of secondary phases and lower energy grain boundaries. As shown in Fig. 8, fracture typically starts as an intermetallic particle failure. Microcracks that start close to the intermetallic particles create the softening phase (Fig. 8b and d). During this fatigue stage, dislocation movements and pileups lead to the onset and nucleation of fractures in intermetallic particles and physically small cracks [38]. The intermetallic particle-induced

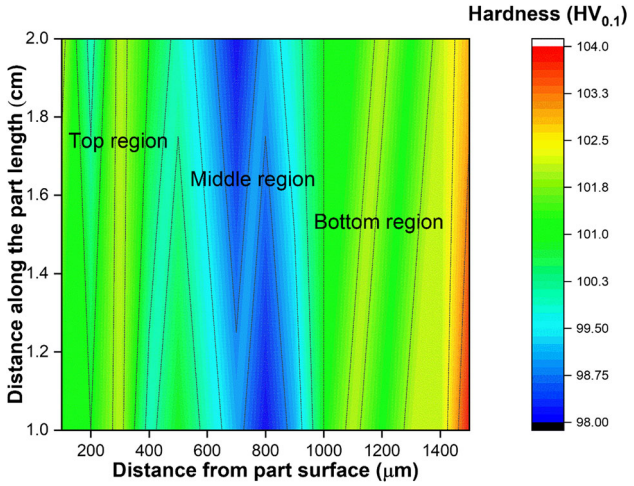

Fig. 6 Contour plot of microhardness of the fabricated part across the cross section

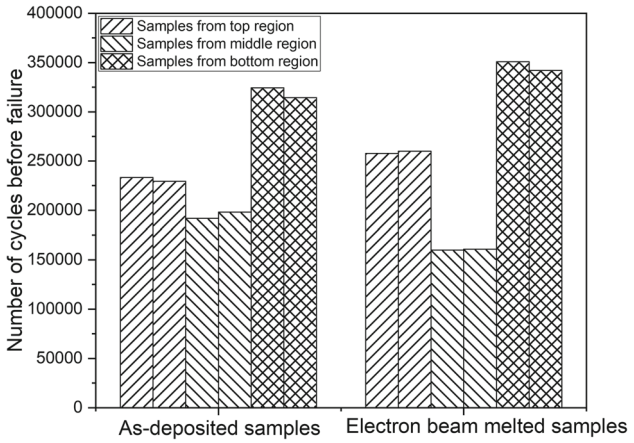

Fig. 7 Fatigue analysis of the samples near the top, bottom, and middle region

crack initiations occur between 15 and 20% before the lifetime of the material. Dimples can be seen on the fractured samples, as seen in Fig. 8a and c. Surface cracks are shown to occur around the top region, even at modest cycle counts. Figure 8b depicts the surface cracks. However, fewer microcracks can be seen in the samples separated near the bottom, which may be attributed to the strengthening phases of the formation.

At the constant stress amplitude, electron beam melted samples showed a higher fatigue life in the top, middle, and bottom regions. This should be attributed to the susceptibility to fatigue cracking at the matrix interface region due to the formation of coarser precipitates. As shown in Fig. 9, due to the remelting with electron beam melting, surface cracks, and material-related defects were reduced. The bonding among the particles became stronger due to the dissolution of secondary phases, which strengthened the matrix phase. The solid solution strengthening restricts the initiation of surface cracks to the formation of secondary cracks (Fig. 9b and d). The electron beam treatment led to stress relief in the composition of the AA7075 alloy. The treatment reduces the fine microstructure obtained during the fabrication and leads to the coarsening and homogenization of the microstructure (Fig. 9c). Several studies revealed that as-deposited parts have a refined microstructure. Post-processing treatments led to the coarsening of grains, which eventually showed better fatigue performance. The electron beam treated sample had better mechanical properties and achieved better fatigue resistance as compared to the untreated alloy. In fact, when the heat-treated material regained its initial strength, the highest stress applied was still below the yield stress of the untreated material, which resulted in a delay in plastic deformation. The irradiated specimens had a higher fatigue life due to the delay in crack initiation, which was a result of the delay in the destruction of the hardened surface layer.

The presence of heterogenous grain structures is crucial for improving fatigue performance. These structures consist of both fine and coarse grains, which can be observed near the subsurface. Due to the higher tortuosity, cracks were stopped from propagating in the fine-grained zone. The formation of these heterogenous grain structures also helped to reduce the potential risk of microcrack initiation, thus further decreasing the possibility of crack propagation.

4 Conclusions

In the present study, additively manufactured AA7075 aluminum alloy was successfully fabricated using the MIG welding technique using constant optimum process parameters. The microstructural and fatigue properties of samples along the width of the AMed part were systematically investigated. The conclusions can be drawn as follows:

1. The fatigue strength of the samples in the middle region decreases by 16% compared to the top region sample due to brittleness, microcracks, and pores. This decrease can be attributed to grain refinement, which results in increased density and stability of the dislocation structure.
2. The microhardness of the bottom region was 13% higher than the middle region due to the formation of strengthening phases resulting from a reduced temperature gradient. On the other hand, the middle region sample had relatively low microhardness, indicating the presence of larger equiaxed grains.
3. During the fatigue test of top-layered specimens, crack growth was mainly attributed to the intermetallic particles and microcracks that formed and cracked the oxide layer

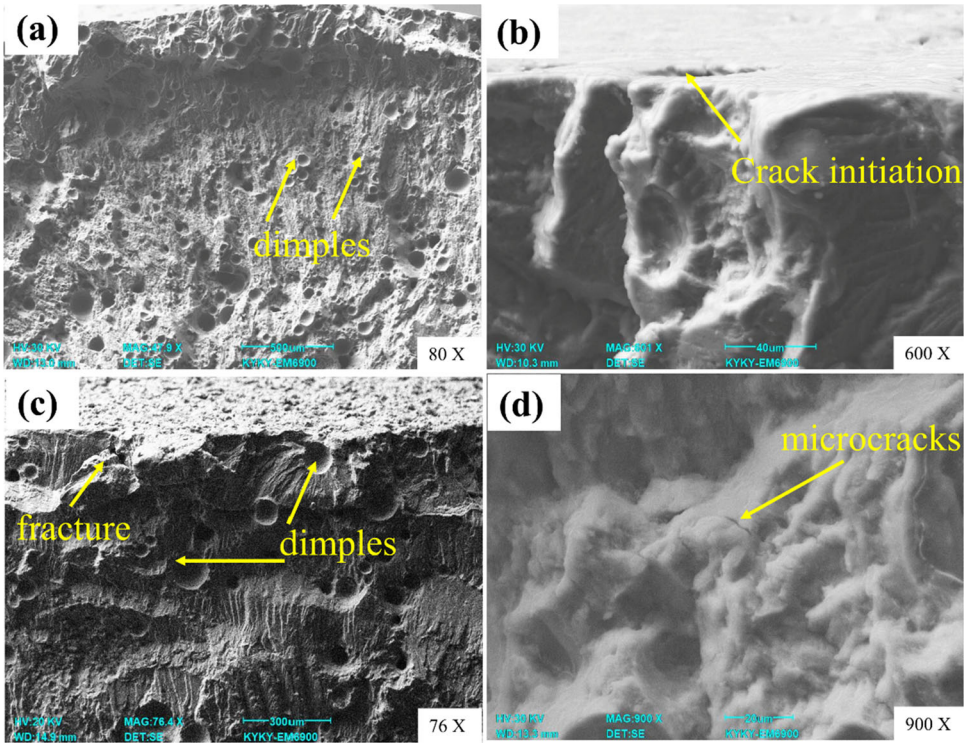

Fig. 8 SEM images of the fractured samples after fatigue test **a**, **b** top region **c**, **d** bottom region

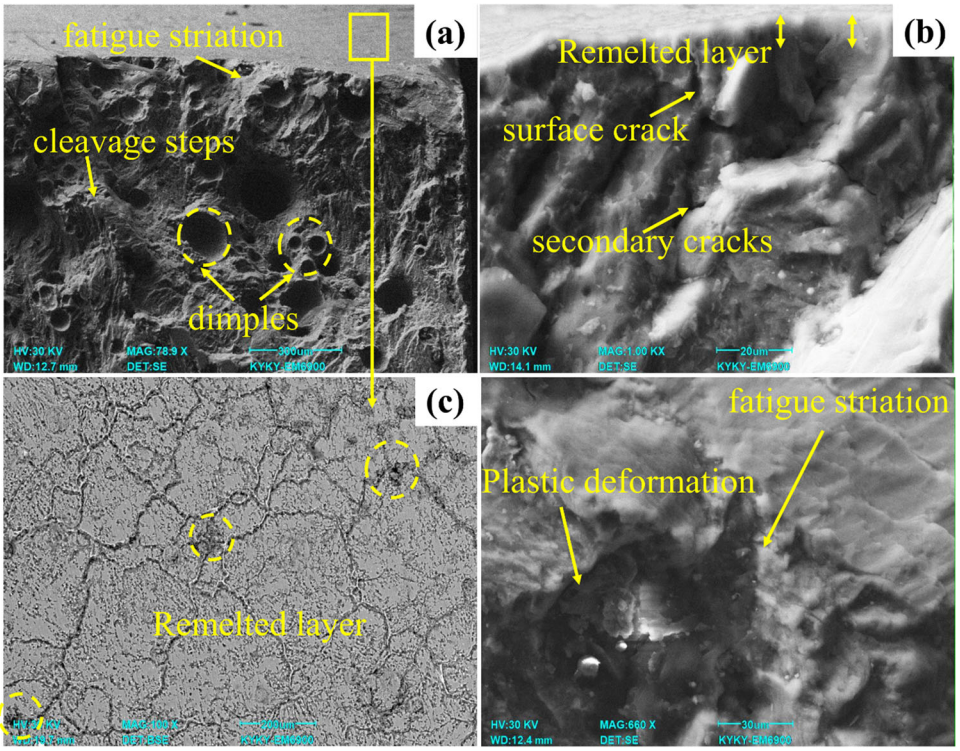

Fig. 9 SEM images of fractured samples of electron beam melted samples after fatigue test **a**, **b** top region **c** microstructure of the surface **d** bottom region

near the surface. However, the occurrence of strengthening phases near the bottom prevented crack growth. This was primarily due to the lower primary dendrite arm spacing in the Aluminum matrix, which had a positive effect throughout the sudden loading.

4. The fatigue life of the electron beam melted samples was found to be 18% higher than that of the as-deposited samples. This was due to the formation of coarse grains and homogenization. The primary characteristic of fatigue crack propagation was ductile fracture, which was accompanied by numerous secondary cracks and occasional fatigue striations. On the other hand, the fracture zone had a prevalence of dimples, which were indicative of ductile fracture.

Funding The work was supported by the Russian Science Foundation, Grant No. 22-79-10245. https://rscf.ru/en/project/22-79-10245/

References

1. Sen, U., Sharma, K.: Friction stir processing of aluminum alloys: a literature survey. **2,** 771–774 (2016)
2. Thangarasu, A., Murugan, N., Dinaharan, I., Vijay, S.J.: Synthesis and characterization of titanium carbide particulate reinforced AA6082 aluminium alloy composites via friction stir processing. Arch. Civ. Mech. Eng **15**, 324–334 (2015)
3. Geng, Y., Panchenko, I., Chen, X., Ivanov, Y., Konovalov, S.: Wire arc additive manufacturing Al-5.0 Mg alloy: microstructures and phase composition. Mater Charact **187**, 111875 (2022). https://doi.org/10.1016/j.matchar.2022.111875
4. Liu, W., Man, Q., Li, J., Liu, L., Zhang, W., Wang, Z., Pan, H.: Microstructural evolution and vibration fatigue properties of 7075–T651 aluminum alloy treated by nitrogen ion implantation. Vacuum **199**(December 2021), 110931 (2022). https://doi.org/10.1016/j.vacuum.2022.110931
5. Su, K., Zhang, J., Li, H., Zeng, D., Yan, T.: Surface & coatings technology effects of the substrate state beneath the coating-substrate interface on fatigue properties of micro-arc oxidation coated 6082–T6 aluminum alloy surf. Coat. Technol. **457**(January 2023), 129274 (2024). https://doi.org/10.1016/j.surfcoat.2023.129274
6. Ivanov, Y.F., Gromov, V.E., Konovalov, S.V., Shliarova, Y.A., Osintsev, K.A., Panchenko, I.A.: Study of the structure and properties of a high-entropy AlCoCrFeNi alloy after electron-beam processing. Phys. Solid State **64**(7), 372–378 (2022). https://doi.org/10.1134/S1063783422080042
7. Gromov, V.E., Shlyarova, Y.A., Ivanov, Y.F., Konovalov, C.V., Vorob'ev, C.V.: Effect of electron beam treatment on the fracture behavior of high-entropy Cr–Mn–Fe–Co–Ni alloy. Met. Sci. Heat Treat. **64**(5), 276–280 (2022). https://doi.org/10.1007/s11041-022-00800-2
8. Gao, H., Zhang, Y., Wu, Q., Song, J., Wen, K.: Fatigue life of 7075–T651 aluminium alloy treated with vibratory stress relief. Int. J. Fatigue **108**(37), 62–67 (2018). https://doi.org/10.1016/j.ijfatigue.2017.11.011
9. da Silva Savonov, G., Camarinha, M.G.G., Rocha, L.O., Barboza, M.J.R., Martins, G.V., Reis, D.A.P.: Study of the influence of the RRA thermal treatment and plasma nitriding on corrosion behavior of 7075–T6 aluminum alloy. Surf. Coat. Technol. **374**, 736–744 (2019). https://doi.org/10.1016/j.surfcoat.2019.04.095
10. Vi, T., Deschanel, S., Godin, N., Normand, B.: On the effect of coatings on the tensile and fatigue properties of 7075–T6 aluminum alloy monitored with acoustic emission (AE): towards lifetime estimation. Int. J. Fatigue **171**(October 2022), 107578 (2023)
11. Huang, X., Qi, H., Li, S., Song, J., Yang, X., Shi, D.: Surface & coatings technology effect of thermal barrier coatings on the fatigue behavior of a single crystal nickel-based superalloy: mechanism and lifetime modeling. Surf. Coat. Technol. **454**(October 2022), 129184 (2023). https://doi.org/10.1016/j.surfcoat.2022.129184
12. Asgaribakhtiari, H., Majzoobi, G.H., Elmkhah, H.: Surface & coatings technology on the effect of Cr/CrN nanolayered coating deposited by arc-PVD method on axial fretting fatigue behavior of Al7075-T6 alloy. Surf. Coat. Technol. **454**(December 2022), 129176 (2023). https://doi.org/10.1016/j.surfcoat.2022.129176
13. Tsai, P.H., Li, T.H., Hsu, K.T., Ke, J.H., Jang, J.S.C., Chu, J.P.: Coating thickness effect of metallic glass thin film on the fatigue-properties improvement of 7075 aluminum alloy. Thin Solid Films **677**(1), 68–72 (2019)
14. Vié, T., Godin, N., Deschanel, S., Normand, B.: On the effect of coatings and pre-corrosion during fatigue tests of 7075-T6 aluminum alloy monitored with acoustic emission (AE). E J. Nondestruct. Test. **28**(1), 107 (2023)
15. Kazanas, P., Deherkar, P., Almeida, P., Lockett, H., Williams, S.: Fabrication of geometrical features using wire and arc additive manufacture. Proc. Inst. Mech. Eng. Part C J. Eng. Manuf. **226**, 1042 (2012)
16. Zhang, Y.M., Li, P.J., Chen, Y.W., Male, A.T.: Automated system for welding-based rapid prototyping. Mechatronics **12**, 27e53 (2002)
17. Zhang, Y.M., Chen, Y.W., Li, P.J., Male, A.T.: Weld deposition-based rapid pro-totyping: a preliminary study. J. Mater. Process. Technol. **135**, 347e357 (2003)
18. Kim, I.S., Son, J.S., Yarlagadda, P.K.D.V.: A study on the quality improvement of robotic GMA welding process. Robot. Comput. Integr. Manuf. **19**, 567e57 (2003)
19. Akula, S., Karunakaran, K.P.: Hybrid adaptive layer manufacturing: an intelligent art of direct metal rapid tooling process. Robot. Comput. Integr. Manuf. **22**, 113e123 (2006)
20. Xiong, J., Zhang, G.J.: Adaptive control of deposited height in GMAW-based layer additive manufacturing. J. Mater. Process. Technol. **214**, 962e968 (2014)
21. Xiong, J., Zhang, G.J., Qiu, Z.L., Li, Y.Z.: Vision-sensing and bead width control of a single-bead multi-layer part: material and energy savings in GMAW-based rapid manufacturing. J. Clean. Prod. **41**, 82e88 (2013)
22. Yang, D.Q., He, C.J., Zhang, G.J.: Forming characteristics of thin-wall steel parts by double electrode GMAW based additive manufacturing. J. Mater. Process. Technol. **227**, 153e160 (2016)
23. Wang, L.F., Sun, J., Yu, X.L., Shi, Y., Zhu, X.G., Cheng, L.Y., Liang, H.H., Yan, B., Guo, L.J.: Enhancement in mechanical properties of selectively laser-melted AlSi10Mg aluminum alloys by T6-like heat treatment. Mater. Sci. Eng. A **734**(January), 299–310 (2018)
24. Ivanov, D., Travyanov, A., Petrovskiy, P., Cheverikin, V., Alekseeva, E., Khvan, A., Logachev, I.: Evolution of structure and properties of the nickel-based alloy EP718 after the SLM Growth and after different types of heat and mechanical treatment. Addit. Manuf. **18**, 269–275 (2017). https://doi.org/10.1016/j.addma.2017.10.015
25. Wang, P., Gammer, C., Brenne, F., Prashanth, K.G., Mendes, R.G., Rümmeli, M.H., Gemming, T., Eckert, J., Scudino, S.: Microstructure and mechanical properties of a heat-treatable Al–3.5Cu–1.5Mg–1Si alloy produced by selective laser melting.

Mater. Sci. Eng. A **711**(October 2017), 562–570 (2018). https://doi.org/10.1016/j.msea.2017.11.063
26. Meid, C., Dennstedt, A., Ramsperger, M., Pistor, J., Ruttert, B., Lopez-Galilea, I., Theisen, W., Körner, C., Bartsch, M.: Effect of heat treatment on the high temperature fatigue life of single crystalline nickel base superalloy additively manufactured by means of selective electron beam Melting. Scr. Mater. **168**, 124–128 (2019). https://doi.org/10.1016/j.scriptamat.2019.05.002
27. Li, J., Cheng, X., Li, Z., Zong, X., Zhang, S.Q., Wang, H.M.: Improving the mechanical properties of Al–5Si–1Cu–Mg aluminum alloy produced by laser additive manufacturing with post-process heat treatments. Mater. Sci. Eng. A **735**(July), 408–417 (2018). https://doi.org/10.1016/j.msea.2018.08.074
28. Deng, D., Peng, R.L., Moverare, J.: On the dwell-fatigue crack propagation behavior of a high strength superalloy manufactured by electron beam melting. Mater. Sci. Eng. A **760**(June), 448–457 (2019). https://doi.org/10.1016/j.msea.2019.06.013
29. Kirka, M.M., Greeley, D.A., Hawkins, C., Dehoff, R.R.: Effect of anisotropy and texture on the low cycle fatigue behavior of Inconel 718 processed via electron beam melting. Int. J. Fatigue **105**, 235–243 (2017). https://doi.org/10.1016/j.ijfatigue.2017.08.021
30. Geng, Y., Panchenko, I., Konovalov, S., Chen, X., Ivanov, Y.: Effect of electron beam energy densities on the surface morphology and tensile property of additively manufactured Al–Mg alloy. Nucl. Instrum. Methods Phys. Res. Sect. B Beam Interact. Mater. Atoms **498**, 15–22 (2021). https://doi.org/10.1016/j.nimb.2021.04.008
31. Liang, R., Huang, C., Liu, F., Liu, F., Lin, X.: Effect of line energy density in repairing 34CrNiMo6 steel by electron beam remelting. J. Manuf. Process. **79**, 314–325 (2022). https://doi.org/10.1016/j.jmapro.2022.04.030
32. Gao, Y.: Surface modification of TC4 titanium alloy by high current pulsed electron beam (HCPEB) with different pulsed energy densities. J. Alloys Compd. **572**, 180–185 (2013). https://doi.org/10.1016/j.jallcom.2013.04.002
33. Li, J., Cheng, X., Li, Z., Zong, X., Chen, X.H., Zhang, S.Q., Wang, H.M.: Microstructures and mechanical properties of laser additive manufactured Al–5Si–1Cu–Mg alloy with different layer thicknesses. J. Alloys Compd. **789**, 15–24 (2019). https://doi.org/10.1016/j.jallcom.2019.03.101
34. Zhang, Z., Sun, C., Xu, X., Liu, L.: Surface Quality and forming characteristics of thin-wall aluminium alloy parts manufactured by laser assisted MIG arc additive manufacturing. Int. J. Light. Mater. Manuf. **1**(2), 89–95 (2018). https://doi.org/10.1016/j.ijlmm.2018.03.005
35. Macek, W., Branco, R., Costa, J.D., Pereira, C.: Strain sequence effect on fatigue life and fracture surface topography of 7075-T651 aluminium alloy. Mech. Mater. **160**(June), 103972 (2021)
36. Pan, X., Zhou, L., Wang, C., Yu, K., Zhu, Y., Yi, M., Wang, L., Wen, S., He, W., Liang, X.: Microstructure and residual stress modulation of 7075 aluminum alloy for improving fatigue performance by laser shock peening. Int. J. Mach. Tools Manuf **184**(June 2022), 103979 (2023). https://doi.org/10.1016/j.ijmachtools.2022.103979
37. Zhang, R., Zhao, W., Zhang, H., Yang, W., Wang, G.X., Dong, Y., Ye, C.: Fatigue performance rejuvenation of corroded 7075–T651 aluminum alloy through ultrasonic nanocrystal surface modification. Int. J. Fatigue **153**(July), 106463 (2021). https://doi.org/10.1016/j.ijfatigue.2021.106463
38. Liu, Z., Zhao, D., Wang, P., Yan, M., Yang, C., Chen, Z., Lu, J., Lu, Z.: Additive manufacturing of metals: Microstructure evolution and multistage control. J. Mater. Sci. Technol. **100**, 224–236 (2022). https://doi.org/10.1016/j.jmst.2021.06.011